Jordan Journal of Mathematics and Statistics (JJMS), 15(2), 2022, pp 211 - 229
DOI: https://doi.org/10.47013/15.2.4

NUMERICAL SOLUTION OF BIOHEAT TRANSFER MODEL USING GENERALIZED WAVELET COLLOCATION METHOD

MOHD IRFAN [1] AND FIRDOUS A. SHAH [2]

Abstract. In this article, we develop a a generalized wavelet collocation method based on a Haar wavelet to facilitate the solution of modified Pennes bio-heat transfer model during thermal therapy. The process of heat transfer in living biological tissue is studied under various coordinate systems. Contrary to the existing operational matrix methods based on orthogonal functions, we construct the Haar wavelet operational matrices of integration without using the block pulse functions. The temperature distribution inside a living biological tissue has been investigated for different estimations of thermal conductivity, antenna power constant, and surface temperature. The numerical results obtained shows that the desired temperature occur faster in spherical symmetric coordinate as compared to axisymmetric coordinate where as temperature in axisymmetric coordinate occur faster in comparison to cartesian coordinate. The performance and accuracy of the proposed technique is elucidates by a comparison of the numerical outcomes with homotopy perturbation method and the exact solution of the model.

1. Introduction

Thermal therapy is a mostly used technique for the treatment of cancer, in which cancer cells are exposed to a significant amount of heat by some external heat source for instance electromagnetic radiation, ultrasound, radio-frequency, microwaves, and infrared radiation. In recent investigations, it has been indicated that cancer cells are relatively more sensitive to heat than normal cells and bringing about their breakdown

2000 *Mathematics Subject Classification.* 42C40, 80M22, 35Q79, 65T60.

Key words and phrases. Bio-heat model; Coordinate system; Haar wavelet; Collocation method; Operational matrices.

Copyright © Deanship of Research and Graduate Studies, Yarmouk University, Irbid, Jordan.

Received: Oct. 12, 2020 Accepted: Dec. 23, 2020 .

at raised temperatures. Based on the level of temperature rise and time to apply them, thermal therapy is arranged into cryoablation ($\theta \leq -50°C$) for time $t >$ 10 min, hyperthermia ($40°C \leq \theta \leq 41°C$) for time $6 - 72$ h, moderate hyperthermia ($41°C \leq \theta \leq 46°C$) for time $15 - 60$ min and thermal ablation ($\theta \geq 50°C$) for time $4 - 6$ min [14]. Heat transfer in living tissues is a complicated process because of their nonhomogeneous internal structure which includes heat conduction in tissues and veins, convection among blood and tissue, perfusion through capillary tubes inside the tissues, metabolic heat generation, and evaporation, and so forth. To demonstrate this intricate process a few bio-heat transfer models have been proposed for an exact prediction and control of temperature [29, 18, 4, 30, 22]. However, because of straightforwardness and clear nature, the Pennes bio-heat transfer model has gained a decent status. Mathematically, the Pennes bio-heat transfer model is depicted by a second order partial differential equation [24]

$$\rho c \frac{\partial \theta}{\partial \zeta} = K_\zeta \frac{\partial^2 \theta}{\partial \eta^2} + \omega_b c_b (\theta_b - \theta) + Q_m + Q_\eta, \tag{1.1}$$

where $\rho, c, K_\zeta, \omega_b, c_b, \theta_b$, and θ represents the density, specific heat, thermal conductivity, blood perfusion rate, specific heat of the blood, arterial temperature, and temperature of the tissue, respectively. To understand the process of heat transfer in living biological tissues, the analytical and numerical study of the Pennes model (1.1) has received great attention from many researchers. Some of the methods invoked in the recent literature for solving the Pennes bio-heat transfer model include the finite difference-decomposition method [10], homotopy perturbation method [11], Monte Carlo method [7], Bessel's method [32], boundary element method [5], variational iteration method [12], Laplace transform method [1] and finite difference method [33].

Wavelet-based numerical algorithms have gained a significant place in numerical analysis fundamentally because of their simple technique, easy calculation, and fast convergence. During the most recent decade, the operational matrices of integration for the Legendre wavelets, Chebyshev wavelets, Haar wavelets, Bernoulli wavelets, CAS wavelets, and the ultraspherical wavelets are constantly being utilized for the solution of various physical and biological problems [15, 16, 25, 26, 2], however, the

Haar wavelets have received unprecedented attention mainly due to their promising features including compact support, real-valued, symmetry and orthogonality [6, 19]. Other distinguishing features of these wavelets include their ability to detect the singular points, a straightforward inclusion of the diverse types of boundary conditions and the possibility to integrate them at arbitrary times [8, 9]. The wavelet techniques have also proved to be successful in managing the numerical solutions of fractional order models. For a detailed survey of the utilization of wavelets techniques in solving fractional order models, we allude to the articles [27, 28].

Keeping in view the pleasant qualities of the Haar wavelets over the other wavelet families, we are profoundly inspired to comprehend the modified bio-heat transfer model by defining a Haar wavelet collocation technique without utilizing the block pulse functions, which is quite unique from the commonly used wavelet-based collocation methods [3, 17]. The proposed technique has the following advantages in contrast to the existing methods available in the open literature:

- The operational matrices of integration are constructed without using the block pulse functions.
- Unlike the conventional methods, our method does not require to calculate the inverse of the Haar matrix.
- The CPU time is significantly curtailed as the major blocks of Haar wavelet operational matrices are calculated once and, are used in the subsequent computations repeatedly.
- Simple and direct relevance with no need for other moderate method is required.

The rest of the paper is sorted out as follows. In Section 2, we introduced the formation of the modified bio-heat transfer model. Section 3 is devoted to the construction of an operational matrix of integration without using the block pulse functions. The solution of the model is illustrated in Section 4. In Section 5, we discuss the achieved numerical results. At last, a conclusion is depicted in Section 6.

2. Mathematical formulation of the model

In this Section, we formulate the modified bioheat transfer model by utilizing the classical Fourier's law of heat conduction in conjunction with the well known energy balance equation. To study the temperature distribution in a living biological tissue, we consider three types of 1D coordinate systems i.e cartesian, axisymmetric, and spherical symmetric coordinate. The classical Fourier law of heat conduction is given by [21]

$$q(\eta,\zeta) = -K_\zeta \frac{\partial \theta}{\partial \eta}, \tag{2.1}$$

where η is space variable, ζ is time variable, and θ is temperature of the tissue. It is notable, that the 1D transient energy balance condition is given by

$$\rho c \frac{\partial \theta}{\partial \zeta} = -\frac{\partial q}{\partial \eta} - \frac{\Gamma}{\eta} q + Q_b + Q_m + Q_\eta, \tag{2.2}$$

where the parameter Γ in (2.2) represents the number which allocates the coordinates i.e., $\Gamma = 0, 1, 2$ specify the cartesian, axisymmetric and spherical symmetric coordinates, respectively (as shown in Fig. 1)[23]. By wiping out q from (2.1) and (2.2), we acquire the following form of modified Pennes bio-heat transfer model

$$\rho c \frac{\partial \theta}{\partial \zeta} = K_\zeta \left(\frac{\partial^2 \theta}{\partial \eta^2} + \frac{\Gamma}{\eta} \frac{\partial \theta}{\partial \eta} \right) + Q_b + Q_m + Q_\eta, \tag{2.3}$$

with initial and boundary conditions as

$$\theta(\eta, 0) = \theta_0, \quad \theta(L_1, t) = \theta_w, \quad \theta(L_2, t) = \theta_s. \tag{2.4}$$

The terms Q_m and Q_b involved in Eqn. (2.3) represents the temperature-dependent heat by metabolic process and heat source because of blood circulation, respectively, and can also be expressed as

$$Q_m = Q_{m1}\left[1 + 0.1(\theta - \theta_0)\right], \text{ and } Q_b = \omega_b c_b \big(\theta_b - \theta\big). \tag{2.5}$$

Moreover, by electromagnetic radiation the heat generated per unit volume of tissue Q_η is given by

$$Q_\eta = \rho S P e^{a(\overline{\eta} - \eta_p)}, \tag{2.6}$$

where a and S are the antenna constants, P is the transmitted power which can be changed as per the prerequisite, $\overline{\eta} = (L - \eta)$ is the distance of the tissue from the skin

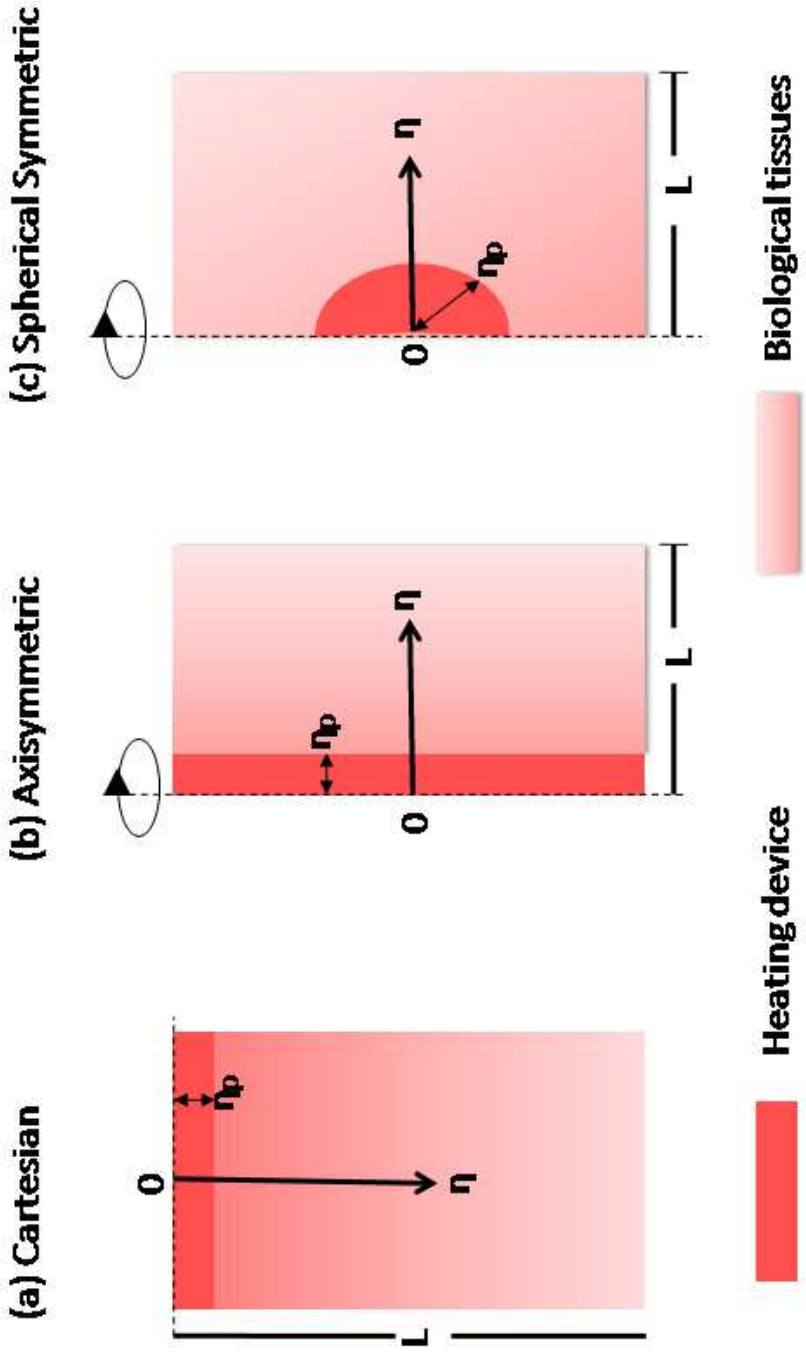

FIGURE 1. Model of bio-heat transfer analysis at distinct coordinates

surface, and η_p is the radius of the probe. After substituting the terms Q_η, Q_m, and Q_b in Eq. (2.3), we obtained the following modified Pennes bio-heat transfer model

$$\frac{\partial\theta}{\partial\zeta} = B\left(\frac{\partial^2\theta}{\partial\eta^2} + \frac{\Gamma}{\eta}\frac{\partial\theta}{\partial\eta}\right) + R\theta(\eta,\zeta) + Z(\eta), \tag{2.7}$$

where

$$B = \frac{K_\zeta}{\rho c}, \quad R = \frac{0.1\left[Q_{m1} - 10\omega_b c_b\right]}{\rho c}, \tag{2.8}$$

and

$$Z(\eta) = \frac{1}{\rho c}\left[Q_{m1} - 0.1Q_{m1}\theta_0 + \omega_b c_b \theta_b + \rho S P e^{a(\overline{\eta}-\eta_p)}\right]. \tag{2.9}$$

3. Haar Wavelets and Operational Matrix of Integration

In 1910, Alfred Haar introduced an orthonormal system for $\mathrm{L}^2[0,1]$ by the combined actions of dyadic dilations and integer translation from a single function, called the Haar wavelet. It is the simplest and oldest orthonormal wavelet with compact support. The fundamental form of the Haar wavelet is the Haar scaling function that presents in the form of a square wave over the interval $\eta \in [0,1]$ as

$$w_0(\eta) = \begin{cases} 1, & \eta \in [0,1] \\ 0, & \text{elsewhere.} \end{cases} \tag{3.1}$$

The above equation represents the zeroth level of wavelet with no translation and dilation of unit size and is known as father wavelet. Corresponding to the father wavelet (3.1), the associated mother wavelet is defined as

$$w_1(\eta) = \begin{cases} 1, & 0 \le \eta < 1/2 \\ -1, & 1/2 \le \eta < 1 \\ 0, & \text{elsewhere.} \end{cases} \tag{3.2}$$

The equation (3.2) can also be written in the linear combination of the Haar scaling function as

$$w_1(\eta) = w(2\eta) - w(2\eta - 1). \tag{3.3}$$

Correspondingly, by translating and dilating the mother wavelet $w_1(\eta)$, we can obtain the other levels of wavelets. For the construction of the Haar wavelets family, the general formula is defined as

$$w_i(\eta) = \begin{cases} 1, & \eta \in [\alpha, \beta) \\ -1, & \eta \in [\beta, \gamma) \\ 0, & \text{elsewhere,} \end{cases} \tag{3.4}$$

where $\alpha = \dfrac{k}{2^j}$, $\beta = \dfrac{k+0.5}{2^j}$, $\gamma = \dfrac{k+1}{2^j}$, the level of wavelet $j = 0, 1 \ldots J$, and translation parameter $k = 0, 1, \ldots, 2^j - 1$. The parameter J is the maximal level of resolution. The index i shows up in (3.4) is obtained via the formula $i = 2^j + k + 1$. The maximal value of i is achieved by $N = 2^{j+1}$. For additional information about the Haar wavelets and their applications, we allude to the monographs [19, 13].

Now we formulate the operational matrix of integration by the Haar wavelets (3.4) for which we follow a similar technique as utilized in [20] and the integral of (3.4) gives us

$$\left.\begin{aligned} \mathbf{P}_{i,1}(\eta) &= \int_0^\eta w_i(\eta)\, d\eta, \\ \mathbf{P}_{i,n+1}(\eta) &= \int_0^\eta \mathbf{P}_{i,n}(\eta)\, d\eta, \\ C_{i,n}(\eta) &= \int_0^1 \mathbf{P}_{i,n}(\eta)\, d\eta, \quad n = 1, 2, \ldots \end{aligned}\right\}. \tag{3.5}$$

The integrals in (3.5) can be assessed systematically by the Haar wavelets (3.4) as

$$\mathbf{P}_{i,n}(\eta) = \begin{cases} 0 & \text{for } \eta \in [0, \alpha) \\ \dfrac{1}{\eta!}(\eta - \alpha)^n & \text{for } \eta \in [\alpha, \beta) \\ \dfrac{1}{\eta!}\big[(\eta - \alpha)^n - 2(\eta - \beta)^n\big] & \text{for } \eta \in [\beta, \gamma) \\ \dfrac{1}{n!}\big[(\eta - \alpha)^n - 2(\eta - \beta)^n + (\eta - \gamma)^n\big], & \text{for } \eta \in [\gamma, 1), \end{cases} \tag{3.6}$$

where $i = 2, 3, \ldots$ and $n = 1, 2, \ldots$. Note that

$$\mathbf{P}_{1,n}(\eta) = \frac{\eta^n}{n!}, \quad C_{1,n}(\eta) = \frac{1}{(n+1)!}, \quad n = 1, 2, \ldots.$$

Now by Haar basis functions, any square-integrable function $f(\eta)$ characterized on $[0, 1]$ can be communicated as

$$f(\eta) = a_0 w_0(\eta) + a_1 w_1(\eta) + \cdots = \sum_{i=0}^{\infty} a_i\, w_i(\eta), \quad \eta \in [0, 1] \tag{3.7}$$

where a_i, $i = 0, 1, 2, \ldots$ are the Haar coefficients and are obtained as

$$a_i = \langle f, w_i \rangle = 2^j \int_0^1 f(\eta)\, w_i(\eta)\, d\eta. \tag{3.8}$$

Even though the equation (3.7) is an infinite series, we can sensibly approximate $f(\eta)$ by utilizing finite terms, if $f(\eta)$ is approximated as a piecewise constant function over

each sub-span; i.e

$$f(\eta) \backsimeq f_N(\eta) = \sum_{i=0}^{N-1} a_i \, w_i(\eta). \tag{3.9}$$

The similar matrix form of the equation (3.9) is as follows

$$\mathbf{F}^T = \mathbf{A}_N^T \, \mathbf{W}_N, \tag{3.10}$$

where $\mathbf{F}$ is the discrete form of the continuous function $f(\eta)$, $\mathbf{A}_N^T = [a_0, a_1, \ldots, a_{N-1}]$ represents the N-dimensional Haar coefficient row vector, and $\mathbf{W}_N$ indicate the Haar wavelet matrix of order $N = 2^{j+1}$ is given as

$$\mathbf{W}_N = \begin{pmatrix} \mathbf{w}_0 \\ \mathbf{w}_1 \\ \vdots \\ \mathbf{w}_{N-1} \end{pmatrix} = \begin{pmatrix} w_{0,0} & w_{0,1} & \ldots & w_{0,N-1} \\ w_{1,0} & w_{1,1} & \ldots & w_{1,N-1} \\ \vdots & \vdots & \vdots & \vdots \\ w_{N-1,0} & w_{N-1,1} & \ldots & w_{N-1,N-1} \end{pmatrix}, \tag{3.11}$$

Any arbitrary function $f(\eta, \zeta) \in L^2([0,1] \times [0,1])$, can be expressed into Haar wavelet series as

$$f(\eta, \zeta) = \sum_{i=0}^{N-1} \sum_{j=0}^{N-1} a_{ij} w_i(\eta) w_j(\zeta), \tag{3.12}$$

where

$$a_{ij} = \langle w_i(\eta), \langle f(\eta, \zeta), w_j(\zeta) \rangle \rangle \,,$$

$$\langle w_i(\eta), w_j(\eta) \rangle = \int_0^1 w_i(\eta) w_j(\eta) \, d\eta. \tag{3.13}$$

We can also write the equation (3.12) as

$$f(\eta, \zeta) = W_N^T(\eta) A W_N(\zeta), \tag{3.14}$$

Following collocation points are defined for achieving the Haar wavelet approximations:

$$\eta_i = \frac{i - 0.5}{N}, \quad i = 1, 2, \ldots, N. \tag{3.15}$$

If we choose $j = 2 \Rightarrow N = 8$, then the corresponding Haar matrix $\mathbf{W}$ and the operational matrix $\mathbf{P}$ can be expressed as

$$\mathbf{W}_8 = \begin{pmatrix} 1 & 1 & 1 & 1 & 1 & 1 & 1 & 1 \\ 1 & 1 & 1 & 1 & -1 & -1 & -1 & -1 \\ 1 & 1 & -1 & -1 & 0 & 0 & 0 & 0 \\ 0 & 0 & 0 & 0 & 1 & 1 & -1 & -1 \\ 1 & -1 & 0 & 0 & 0 & 0 & 0 & 0 \\ 0 & 0 & 1 & -1 & 0 & 0 & 0 & 0 \\ 0 & 0 & 0 & 0 & 1 & -1 & 0 & 0 \\ 0 & 0 & 0 & 0 & 0 & 0 & 1 & -1 \end{pmatrix}, \mathbf{P}_8 = \frac{1}{64} \begin{pmatrix} 32 & -16 & -8 & -8 & -4 & -4 & -4 & -4 \\ 16 & 0 & -8 & 8 & -4 & -4 & 4 & 4 \\ 4 & 4 & 0 & 0 & -4 & 4 & 0 & 0 \\ 4 & 4 & 0 & 0 & -4 & 4 & 0 & 0 \\ 1 & 4 & 2 & 0 & 0 & 0 & 0 & 0 \\ 1 & 1 & -2 & 0 & 0 & 0 & 0 & 0 \\ 1 & -1 & 0 & 2 & 0 & 0 & 0 & 0 \\ 1 & -1 & 0 & -2 & 0 & 0 & 0 & 0 \end{pmatrix}.$$

The Haar approximation $f_N(\eta)$ for a function $f(\eta)$ is given by

$$f_N(\eta) = \sum_{i=0}^{N-1} a_i \, w_i(\eta), \quad N = 2^{j+1}, \; j = 0, 1, 2, \ldots, J \tag{3.16}$$

and also the corresponding N-th level error is given by

$$\left\| f - f_N \right\|_2 = \left\| f(\eta) - \sum_{i=0}^{N-1} a_i \, w_i(\eta) \right\|_2 = \left\| \sum_{i=2^{j+1}}^{\infty} a_i \, w_i(\eta) \right\|_2 . \tag{3.17}$$

We obtain the upper bound of the error for a solution of model (2.7) if we have an exact solution of the model (2.7) at hand. Besides the convergence of the proposed technique might be examined on similar lines as discuss in Yi and Huang [31].

Theorem 3.1. ([31]) *Suppose $f(\eta)$ satisfies the Lipschitz condition on $[0, 1]$ with Lipschitz constant K and $f_N(\eta)$ is the Haar approximation of $f(\eta)$, then we have*

$$\left\| f - f_N \right\|_2 \leq \frac{K}{\sqrt{3}\, N^2} \tag{3.18}$$

4. Method of Solution

This Section is committed for solving the modified bio-heat transfer model (2.7) by employing the Haar wavelet operational matrices technique formulated in Section 3. To encourage the solution of the problem (2.7), we review the non-dimensional model (2.7)

$$\frac{\partial \theta}{\partial \zeta} = B \left(\frac{\partial^2 \theta}{\partial \eta^2} + \frac{\Gamma}{\eta} \frac{\partial \theta}{\partial \eta} \right) + R\theta(\eta, \zeta) + Z(\eta), \tag{4.1}$$

with initial and boundary conditions

$$\theta(\eta, 0) = u(\eta), \quad \theta(0, \zeta) = v_1(\zeta), \quad \theta(L, \zeta) = v_2(\zeta), \tag{4.2}$$

where B, R and $Z(\eta)$ have usual meaning as given in Eqns (2.8) and (2.9).

Next, by the expansion of Haar wavelet, we approximate the highest order derivative $\dfrac{\partial^3\theta}{\partial\eta^2\partial\zeta}$ in the following form

$$\frac{\partial^3\theta}{\partial\eta^2\partial\zeta} \approx W_N^T(\eta)AW_N(\zeta). \tag{4.3}$$

Now by taking the one time integration of (4.3), w.r.t ζ and twice integration w.r.t η, we get

$$\begin{aligned}\frac{\partial^2\theta}{\partial\eta^2} &= \int_0^\zeta \frac{\partial^3\theta}{\partial\eta^2\partial\zeta}d\zeta + \frac{\partial^2\theta}{\partial\eta^2}\Big|_{\zeta=0}\\ &\approx \int_0^\zeta \Big[W_N^T(\eta)AW_N(\zeta)\Big]d\zeta + \frac{\partial^2\theta}{\partial\eta^2}\Big|_{\zeta=0}\\ &= W_N^T(\eta)AP_{i,1}W_N(\zeta) + u^{''}(\eta) \qquad (4.4)\end{aligned}$$

and

$$\begin{aligned}\frac{\partial\theta}{\partial\zeta} &= \int_0^\eta\int_0^\eta \frac{\partial^3\theta}{\partial\eta^2\partial\zeta}d\eta + \eta\frac{\partial\theta}{\partial\zeta}\Big|_{\eta=0} + \frac{\partial\theta}{\partial\zeta}\Big|_{\eta=0}\\ &\approx \int_0^\eta\int_0^\eta \Big[W_N^T(\eta)AW_N(\zeta)\Big]d\eta + \eta\frac{\partial\theta}{\partial\zeta}\Big|_{\eta=0} + \frac{\partial\theta}{\partial\zeta}\Big|_{\eta=0}\\ &= [P_{i,2}W_N(\eta)]^T AW_N(\zeta) + \eta v_1^{'}(\zeta) + v_1^{'}(\zeta). \qquad (4.5)\end{aligned}$$

Upon integrating (4.4), with respect to η from 0 to η, we get

$$\begin{aligned}\frac{\partial\theta}{\partial\eta} &= \int_0^\eta \frac{\partial^2\theta}{\partial\eta^2}dx + \frac{\partial\theta}{\partial\eta}\Big|_{\zeta=0}\\ &\approx \int_0^\eta \Big[W_N^T(\eta)AP_{i,1}W_N(\zeta)\Big]d\eta + \frac{\partial\theta}{\partial\eta}\Big|_{\zeta=0}\\ &= [P_{i,1}W_N(\eta)]^T AP_{i,1}W_N(\zeta) + u^{'}(\eta) \qquad (4.6)\end{aligned}$$

Again integrating (4.5), with respect to ζ from 0 to ζ, we get

$$\begin{aligned}\theta(\eta,\zeta) &= \int_0^\zeta \frac{\partial\theta}{\partial\zeta}d\zeta + \frac{\partial\theta}{\partial\zeta}\Big|_{\zeta=0}\\ &\approx \int_0^\zeta \Big[\,[P_{i,2}W_N(\eta)]^T AW_N(\zeta) + \eta v_1^{'}(\zeta) + v_1^{'}(\zeta)\Big]d\zeta + \frac{\partial\theta}{\partial\zeta}\Big|_{\zeta=0}\\ &= [P_{i,2}W_N(\eta)]^T AP_{i,1}W_N(\zeta) + \eta v_1(\zeta) + v_1(\zeta) + u(\eta). \qquad (4.7)\end{aligned}$$

Substituting the obtained values of $\frac{\partial^2\theta}{\partial\eta^2}, \frac{\partial\theta}{\partial\zeta}, \frac{\partial\theta}{\partial\eta}, \theta(\eta,\zeta)$, in (4.1), we obtain the algebraic equations in the following form

$$[P_{i,2}W_N(\eta)]^T AW_N(\zeta) - BW_N^T(\eta)AP_{i,1}W_N(\zeta) - B\frac{\Gamma}{\eta}[P_{i,1}W_N(\eta)]^T AP_{i,1}W_N(\zeta) - R[P_{i,2}W_N(\eta)]^T AP_{i,1}W_N(\zeta)$$

$$= Z(\eta) + \eta v_1(\zeta) + v_1(\zeta) + u(\eta) + B\frac{\Gamma}{\eta}u'(\eta) + B + u''(\eta) - \eta v_1'(\zeta) - v_1'(\zeta). \tag{4.8}$$

Upon solving the above algebraic equation (4.8) with the help of Newton's method, we get the values of our unknown Haar coefficient vector A. Then putting the attain values of vector A in (4.7), we get our approximate solution $\theta(\eta,\zeta)$ of modified bioheat transfer model (4.1).

4.1. **Exact Solution of the model.** To check the performance and accuracy of the present technique an exact solution is required. It is not possible to obtain the exact solution of the proposed model (2.7), so to achieve this we curtail the model into a more simple form by setting the model into cartesian coordinate i.e $\Gamma = 0$ with initial and boundary conditions as given in (2.4), and then using the Laplace transforms technique, the exact solution of the model (2.7) comes out to be [11]

$$\begin{aligned}
\theta(\eta,\zeta) = {} & \frac{1}{\sinh\left(\sqrt{d_1}(L_2-L_1)\right)} \\
& \times \left[\left\{\theta_w - \frac{U_0}{d_1} - \frac{U_1}{(d_1-a^2)}\left(1 - \sinh\frac{\sqrt{a}(L_2-\eta)}{\sinh(\sqrt{d_1}(L_2-\eta))}\exp\left(\frac{-(d_1-a^2)}{d_2}\zeta\right)\right)\right\}\right. \\
& \times \sinh(\sqrt{d_1}(L_2-\eta)) + \left\{\theta_s - \frac{U_0}{d_1} - \frac{U_2}{(d_1-a^2)}\right. \\
& \times \left.\left.\left(1 - \frac{\sinh(\sqrt{a}(L_2-\eta))}{\sinh(\sqrt{d_1}(L_2-\eta))}\exp\left(\frac{-(d_1-a^2)}{d_2}\zeta\right)\right)\right\}\sinh\left(\sqrt{d_1}(L_2-\eta)\right)\right] \\
& - \frac{U_0}{d_2}\exp\left(-\frac{d_1}{d_2}\zeta\right) - \frac{\rho c\theta_0}{K_\zeta d_2}\exp\left(-\frac{d_1}{d_2}\zeta\right) + \frac{\rho SP\exp\left(a(0.04-\eta)\right)}{K_\zeta\left(d_1-a^2\right)} \\
& \times \left\{1 + \exp\left(-\frac{(d_1-a^2)}{d_2}\zeta\right)\right\} - \frac{\rho c\theta_0}{K_\zeta d_1}\exp\left(-\frac{d_1}{d_2}\zeta\right) + \frac{1}{K_\zeta d_1}\left(Q_{m1}\right. \\
& \left. - \frac{Q_{m1}}{10}\theta_0' + \omega_b c_b\theta_b\right) \times \left\{1 - \exp\left(-\frac{d_1}{d_2}\zeta\right)\right\} + \sum_{n=1}^{\infty}\left[\frac{2(-1)^n}{(n^2\pi^2 + d_1(L_2-L_1)^2)}\right. \\
& \times \left\{\left(n\pi\theta_w + \frac{1}{n\pi} + \frac{n\pi}{(n^2\pi^2 + a^2(L_2-L_1)^2)} - \frac{\rho c\theta_0\left(n^2\pi^2 + d_1(L_2-L_1)^2\right)}{n\pi K_\zeta d_2}\right)\right.
\end{aligned}$$

$$\times \left(\sin\left(\frac{n\pi(L_2-\eta)}{(L_2-L_1)}\right)+\left(n\pi\theta_s+\frac{1}{n\pi}+\frac{n\pi}{(n^2\pi^2+a^2(L_2-L_1)^2)}\right.\right.$$
$$\left.\left.-\frac{\rho c\theta_0\left(n^2\pi^2+d_1(L_2-L_1)^2\right)}{n\pi K_\zeta d_2}\right)\right)\sin\left(\frac{n\pi(\eta-L_1)}{(L_2-L_1}\right)\Bigg\}$$
$$\times\exp\left\{-\frac{\zeta}{d_2}\left(d_1+\frac{n^2\pi^2}{(L_2-L_1)^2}\right)\right\}\Bigg], \text{where} \tag{4.9}$$
$$d_1=\frac{1}{K_\zeta}\left(\omega_b c_b-0.1Q_{m1}\right),\ d_2=\frac{\rho c}{K_\zeta},\ U_0=\frac{1}{K_\zeta}\left(Q_{m1}-0.1Q_{m1}\theta_0^{'}+\omega_b c_b\theta_b\right),$$
$$U_1=\frac{\rho SP}{K_\zeta}e^{(a(0.04-L_1))},\ U_2=\frac{\rho SP}{K_\zeta}e^{(a(0.04-L_2))}.$$

5. Discussion of the numerical results

In this section, we introduce and talk about the numerical results of the proposed technique for solving the modified bio-heat transfer model (2.7). The values of the parameters for thermophysical properties of living biological tissue and blood utilized in this paper are listed in Table 1, whereas source parameters are listed in Table 2. To test the performance and accuracy of the present technique, we present a tabulated and graphical comparison of our acquired numerical results with those of the results attained by the Homotopy perturbation method [11] and exact solution for the Cartesian coordinate system as depicted in Table 3 and Figure 2. It is quite evident from Table 3 and Figure 2, that our numerical solution behaves much better and is sensibly nearer to the solution obtained by HPM and exact solution (4.9). Moreover, in Table 3 we also present the effect of metabolic heat generation Q_m on the temperature distribution of living biological tissues.

Table 1. Parameters for thermophysical properties of tissue and blood utilized in this paper.

Parameters	Values	Units	Refs.
c	4.18×10^3	$Jkg^{-1}K^{-1}$	[10]
ρ	1×10^3	kgm^{-1}	[10]
K_ζ	0.5	Wm^{-1}	[10]
ω_b	8	$kgm^{-3}s^{-1}$	[10]
c_b	3.344×10^3	$Jkg^{-1}K^{-1}$	[10]
P	20	W	[11]

Parameters	Values	Units	Refs.
Q_{m1}	1.091×10^3	Wm^{-3}	[10]
θ_s	20	$^\circ C$	[11]
θ_w	37	$^\circ C$	[11]
θ_a	37	$^\circ C$	[11]
θ_0	37	$^\circ C$	[11]
L_1	1×10^{-3}	m	[11]
L_2	5×10^{-2}	m	[11]
L	0.05	m	[11]

TABLE 2. The parameters of constant source term utilized in this paper..

Parameters	Values	Units	Refs.
a	-127	m^{-1}	[11]
S	12.5	kg^{-1}	[11]
η_p	0.01	m	[11]

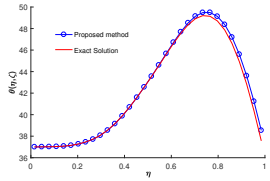

FIGURE 2. Comparison between Proposed method and Exact Solution

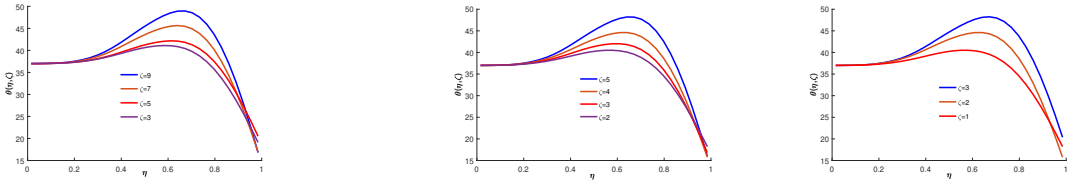

(a) (b) (c)

FIGURE 3. (a) Plot of $\theta(\eta, \zeta)$ vs. η at different time ζ for $\Gamma = 0$. (b) Plot of $\theta(\eta, \zeta)$ vs. η at different time ζ for $\Gamma = 1$. (c) Plot of $\theta(\eta, \zeta)$ vs. η at different time ζ for $\Gamma = 2$.

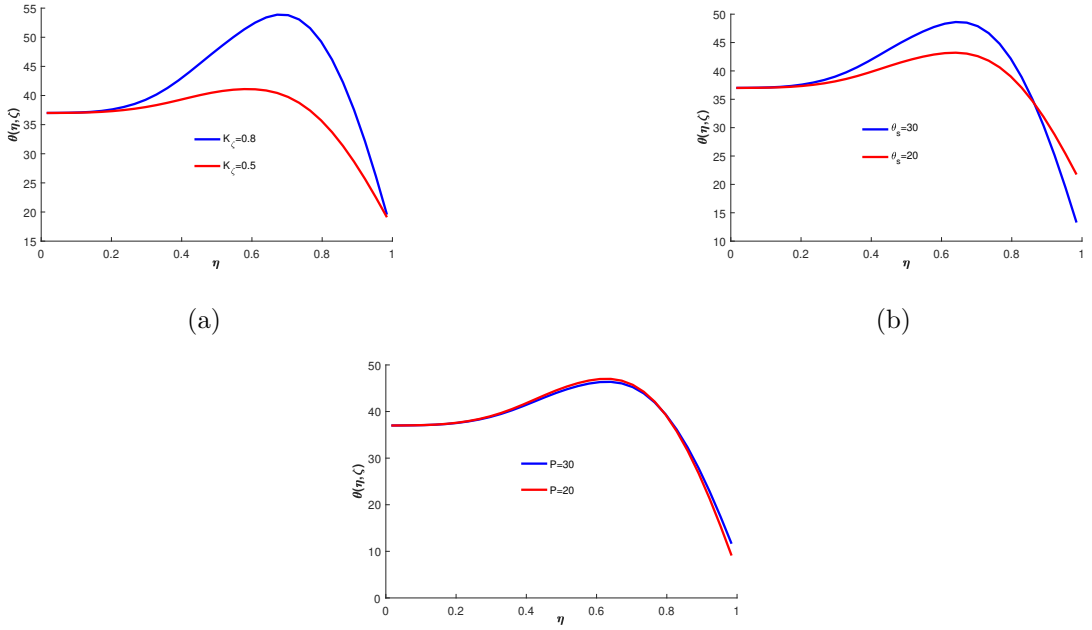

FIGURE 4. (a) Plot of $\theta(\eta, \zeta)$ vs. η at different K_ζ for $\zeta = 9$ min in $\Gamma = 0$. (b) Plot of $\theta(\eta, \zeta)$ vs. η at different θ_s for $\zeta = 9$ min in $\Gamma = 0$. (c) Plot of $\theta(\eta, \zeta)$ vs. η at different P for $\zeta = 9$ min in $\Gamma = 0$.

TABLE 3. Comparision of present technique with HPM [11] under the effects of the metabolic heat generation term (Q_m).

	Temperature$(^\circ C)(Q_m \neq 0)$		Temperature$(^\circ C)(Q_m = 0)$	
Distance(η)				
	HWCM	**HPM**[11]	**HWCM**	**HPM**[11]
0.01	37.00	37.00	37.00	37.00
0.59	37.2682	39.9400	37.9673	39.9380
1.08	38.0695	41.7474	39.3283	41.7448
1.57	39.1437	44.3789	40.5378	44.3763
2.06	41.5292	47.7575	42.9272	47.7550
2.55	45.9773	50.5935	45.0106	50.5909
3.04	48.9125	51.2047	46.9526	51.2022
3.53	48.1442	48.3347	48.2938	48.3355

	Temperature($^\circ C$)($Q_m \neq 0$)		Temperature($^\circ C$)($Q_m = 0$)	
Distance(η)				
	HWCM	**HPM**[11]	**HWCM**	**HPM**[11]
4.02	43.6398	41.9886	42.8366	41.9870
4.51	32.7671	34.2236	34.5278	34.2229
5.00	20.00	30.00	20.00	30.00

The temperature distributions in living tissue during thermal therapy for three coordinates system i.e ($\Gamma = 0, 1$ & 2) is shown graphically in Figure 3 and we infer from Figure 3 that desired temperature occur faster in spherical symmetric coordinate as compared to axisymmetric coordinate where as temperature in axisymmetric coordinate occur faster in comparison to Cartesian coordinate. The thermal conductivity (K_ζ), antenna power constant (P), and the surface temperature (θ_s) has significant characteristic features on the modified heat transfer model (2.8). To examine the impact of thermal conductivity (K_ζ), antenna power constant (P), and surface temperature (θ_s) on living biological tissue, the temperature profiles for various estimations of K_ζ, θ_s and P are shown in Figs 4. It is clear from Figure 4, that with an increase in the estimations of K_ζ and θ_s, the temperature distribution increases at the location of the tissue. Moreover, with a decrease in the value of antenna power constant (P) from $30^\circ C$ to $20^\circ C$, the temperature distribution shows a small reduction in its behavior at tissue location which is of significant importance for thermal treatment. Finally, in Figure 5, we present the three-dimensional graphs of our approximate solution for different levels of resolution $J = 2; J = 3; J = 4$ and $J = 5$. Figure 5, shows that as the level of resolution J increases the numerical solution appreciably refined and achieve the desired temperature. The numerical results demonstrate that the underlying technique is an impressive and significant tool for study the heat transfer process during thermal therapy.

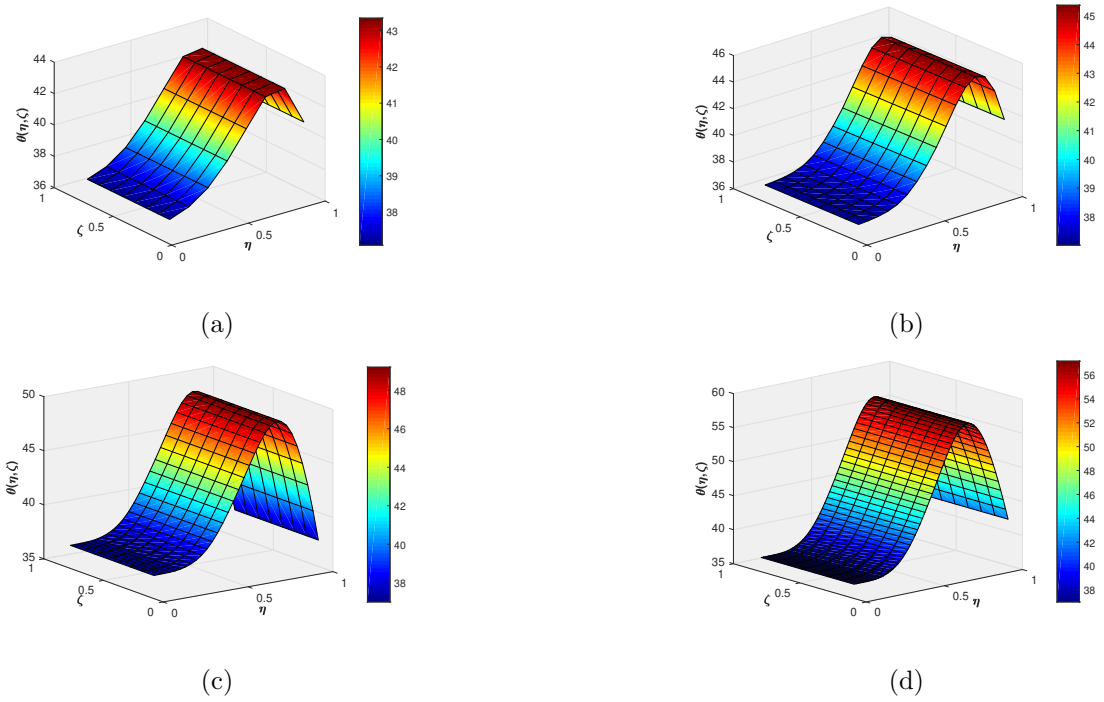

FIGURE 5. Three-dimensional plot of numerical solution for different level of resolution (a) J = 2, (b) J = 3, (c) J = 4 and (d) J = 5.

6. Conclusion

In this article, a collocation method based on Haar wavelets is developed for solving the modified Pennes bio-heat transfer model during thermal therapy. Unlike the existing operational matrix methods based on orthogonal functions, we construct the Haar wavelet operational matrices of integration without using the block pulse functions. By utilizing the proposed technique, we may conclude that this technique is more convenient and efficient for obtaining the numerical solutions of said model (2.7). Moreover, in this study, we also see the effects of thermal conductivity (K_ζ), antenna power constant (P), and the surface temperature (θ_s) on the temperature distribution in living biological tissue. Therefore, the obtained results helps in precise prediction and control of temperature during thermal therapy. The computational process has been carried out in MATLAB(R2019b) software.

References

[1] H. Ahmadikia, R. Fazlali and A. Moradi, Analytical solution of the parabolic and hyperbolic heat transfer equations with constant and transient heat conditions on skin tissue. Int Commun Heat Mass Transfer. 39, 121-130, 2012.

[2] I. Awana and F.A. Shah, An efficient Haar wavelet collocation method for solving Pennes bioheat transfer model, Acta Universitatis Apulensis, 60, 75-89, 2019.

[3] A. Azizi, S. Abdi and J. Saeidian, Applying Legendre wavelet method with Tikhonov regularization for one-dimensional time-fractional diffusion equations. Comp. Appl. Math. 37, 4793-4804, 2018.

[4] M.M. Chen, and M.M. Holmes, Microvascular contributions in tissue heat transfer, Annals of the New York Academy of Sciences, 335, 137-150, 1980.

[5] C.L. Chan, Boundary element method analysis for the bioheat transfer equation. J Biomech Eng 114, 358-365, 1992.

[6] C.F. Chen, and C.H. Hsiao, Haar wavelet method for solving lumped and distributed-parameter systems, IEE Proc. Control Theory Appl., 144, 87-94, 1997.

[7] Z.S. Deng, and J. Liu, Monte Carlo method to solve multi-dimensional bioheat transfer problem. Numer. Heat Transfer Part B: Fundam. 42, 543-567, 2002.

[8] L. Debnath, and F.A. Shah, *Wavelet Transforms and Their Applications*, New York: Birkhäuser, 2015.

[9] L. Debnath, and F.A. Shah, *Lecture notes on Wavelet Transforms*, New York: Birkhäuser, 2017.

[10] P.K. Gupta, J. Singh and K.N. Rai, Solution of the heat transfer problem in tissues during hyperthermia by finite difference-decomposition method. J Appl Math Comput 219(2013), 6882-6892.

[11] P.K. Gupta, J. Singh, and K.N. Rai, Numerical simulation for heat transfer in tissues during thermal therapy, J. Therm. Biol., 35(6), 295-301, 2010.

[12] P.K. Gupta, J. Singh and K.N. Rai, A numerical study on heat transfer in tissues during hyperthermia. Math Comput Model 57, 1018-1037, 2013.

[13] J.S. Gu, and W.S. Jiang, The Haar wavelets operational matrix of integration, Int. J. Syst. Sci., 27, 623-628, 1996.

[14] R.W.Y. Habash, R. Bansal, D. Krewski, and H.T. Alhafid, Thermal therapy, part 1: an introduction to thermal therapy, Crit. Rev. Biomedic. Eng. 34(6), 459-489, 2006.

[15] M.H. Heydari, M.R. Hooshmandasl, C. Cattani, and L. Ming, Legendre Wavelets Method for Solving Fractional Population Growth Model in a Closed System, Mathematical Problems in Engineering, Article ID 161030, 8 pages, 2013.

[16] G. Hariharan, and K. Kannan, Review of wavelet methods for the solution of reaction-diffusion problems in science and engineering, Applied Mathematical Modelling, 38(3), 799-813, 2014.

[17] G. Hariharan and K. Kannan, An overview of Haar wavelet method for solving differential and integral equations, World Applied Sciences Journal 23(12), 01-14, 2013.

[18] H.G. Klinger, Heat transfer in perfused biological tissue-I, Bull. Math. Bio. 36, 403-415, 1974.

[19] U. Lepik, and H. Hein, *Haar Wavelets with their Applications*, New York: Springer, 2014.

[20] U. Lepik, Solving integral and differential equations by the aid of nonuniform Haar wavelets, Appl. Math. Comput., 198, 326-332, 2008.

[21] K. Mitra, S. Kumar, A. Vedavarz, and M.K. Moallemi, Experimental evidence of hyperbolic heat conduction in processed meat, ASME J. Heat Transf. 117, 568-573, 1995.

[22] F. Nakayama, and Kuwahar, A general bioheat transfer model based on the theory of porous media, Int. J. Heat Mass Transfer, 51, 3190-3199, 2008.

[23] J. Okajima, S. Maruyama, H. Takeda, and A. Komiya. Dimensionless solutions and general characteristics of bioheat transfer during thermal therapy. J. Therm. Biol. 34, 377-384, 2009.

[24] H.H Pennes, Analysis of tissue and arterial blood temperature in the resting forearm, J. Appl. Physiol. 1, 93-122, 1948.

[25] P.K. Sahu, and S.R. Saha, A new Bernoulli wavelet method for accurate solutions of nonlinear fuzzy Hammerstein-Volterra delay integral equations, Fuzzy Sets and Systems, 309, 131-144, 2017.

[26] F.A. Shah, and M.I. Awana, A computational wavelet method for solving dual-phase-lag model of bioheat transfer during hyperthermia treatment, Comp. and Math. Methods, 2(4), e1095, 2020, https://doi.org/10.1002/cmm4.1095.

[27] F.A. Shah, and M. Irfan, Generalized Wavelet Method for Solving Fractional Bioheat Transfer Model During Hyperthermia Treatment, Int. J. of Wavelets, Multi. and Inf. Proc., doi.org/10.1142/S0219691320500903.

[28] H.M. Srivastava, F.A. Shah, and M. Irfan, Generalized wavelet quasilinearization method for solving population growth model of fractional order, Math. Meth. Appl. Sci., 1-10, 2020.

[29] W. Wulff, The energy conservation equation for living tissues, IEEE Trans. Biomed. Eng., 21, 494-495, 1974.

[30] S. Weinbaum, L.M. Jiji, and D.E. Lemons, Theory and experiment for the effect of vascular microstructure on surface tissue heat transfer-I, ASME J. of Biomech. Eng., 106, 321-330, 1984.

[31] M. Yi, and J. Huang, Wavelet operational matrix method for solving fractional differential equations with variable coefficients, Appl. Math. Comput., 230, 383-394, 2014.

[32] K. Yue, X. Zhang, and F. Yu, An analytic solution of one-dimensional steady-state Pennes bioheat transfer equation in cylindrical coordinates. J Therm Sci 13, 255-258, 2004.

[33] J.J. Zhao, J. Zhang, N. Kang and F. Yang, A two level finite difference scheme for one dimensional Pennes bioheat equation. Appl Math Comput 171, 320-331, 2005.

(1) Department of Mathematics, University of Kashmir, South Campus, Anantnag-192101, Jammu and Kashmir, India.
Email address: irfan.scholar@kashmiruniversity.net

(2) Department of Mathematics, University of Kashmir, South Campus, Anantnag-192101, Jammu and Kashmir, India.
Email address: fashah@uok.edu.in